

Full-Field Electronic Dispersion Compensation of a 10Gbit/s OOK Signal over 4×124km Field-Installed Single-Mode Fibre

Mary E. McCarthy, Jian Zhao, Andrew D. Ellis, Paul Gunning

Abstract— We experimentally demonstrate the use of full-field electronic dispersion compensation (EDC) to achieve a bit error rate of 5×10^{-5} at 22.3dB optical signal-to-noise ratio for single-channel 10Gbit/s on-off keyed signal after transmission over 496km field-installed single-mode fibre with an amplifier spacing of 124km. This performance is achieved by designing the EDC so as to avoid electronic amplification of the noise content of the signal during full-field reconstruction. We also investigate the tolerance of the system to key signal processing parameters, and numerically demonstrate that single-channel 2160km single mode fibre transmission without in-line optical dispersion compensation can be achieved using this technique with 80km amplifier spacing and optimized system parameters.

Index Terms— Electronic dispersion compensation, chromatic dispersion, detection, asymmetric Mach-Zehnder interferometer

I. INTRODUCTION

Recently, the advance of high-speed microelectronics, such as 25GSamples/s analogue to digital converters (ADC)[1], has enabled the application of electronic dispersion compensation (EDC) in optical communication systems at 10Gbit/s. Compared to its optical counterpart, it is more flexible, cost-effective, and easier to integrate into transmitters or receivers for extending the reach of legacy multimode optical fibre links [2] as well as metro and long-haul optical transmission systems [3-6]. Receiver-side EDC, which can adapt quickly to changes in link conditions, is of particular value for future transparent optical networks where the reconfiguration of the add- and drop-nodes will cause the transmission paths to vary. However, the performance of conventional EDC using direct detection (DD EDC) is limited by the loss of the signal phase information. In addition, the transformation of linear optical impairments arising from chromatic dispersion (CD) into

nonlinear impairments after square-law detection notably increases the operational complexity of the DD EDC. EDC based on coherent detection can access both the intensity and the phase of the optical field, thus allowing full CD compensation. However, it requires additional tight-specification optical components, and signal polarisation and phase tracking or recovery [7,8].

Recently, a novel cost-effective EDC receiver for on-off keyed (OOK) systems was proposed, which accesses the full optical field with significantly reduced complexity using a single asymmetric Mach-Zehnder interferometer (AMZI) prior to photo-detection [9]. The recovered information allows for full optical-field CD compensation with a dispersive transmission line [9-11], feed-forward equalizer [3], or maximum likelihood sequence estimation [12-13] in the electrical domain. In an OOK based system using a dispersive transmission line, the method was experimentally verified to successfully recover a 10Gbit/s signal after transmission over 372km of field-installed standard single-mode fibre (SSMF) [11]. However, the experimental setup was not optimized in this system, so the amplified spontaneous emission (ASE) noise and receiver thermal noise severely degraded the performance. The impact of the noise was further increased by noise amplification mechanisms arising from the division by total received power and low-frequency component amplification in full-field reconstruction [10].

In this paper, we investigate the noise sensitivity of the full-field EDC scheme, and experimentally demonstrate significant performance improvement compared to our previous work [11]. The tolerance of the system to critical signal processing parameters is also investigated, revealing the interdependencies between these parameters. We also report numerical simulations which provide guidelines for further performance improvement, and demonstrate the feasibility of 10Gbit/s OOK transmission over 2160km of SSMF without need for optical dispersion compensation.

The paper is organized as follows: we will present the principle of full field EDC in Section II and describe the experimental setup in Section III. The experimental results are depicted in Section IV, including the analysis of key parameters in off-line signal processing and the system

Manuscript received April 6 2009. This work was supported in part by Science Foundation Ireland under grant number 06/IN/1969.

Mary E. McCarthy, Jian Zhao, and Andrew D. Ellis are with Photonic Systems Group, Tyndall National Institute and Department of Physics, University College Cork, Lee Maltings, Prospect Row, Cork, Ireland. (e-mail: mary.mccarthy@tyndall.ie, jian.zhao@tyndall.ie, andrew.ellis@tyndall.ie).

Paul Gunning is with Futures Testbed, BT Design, Martlesham Heath, Ipswich, UK (e-mail: paul.gunning@bt.com).

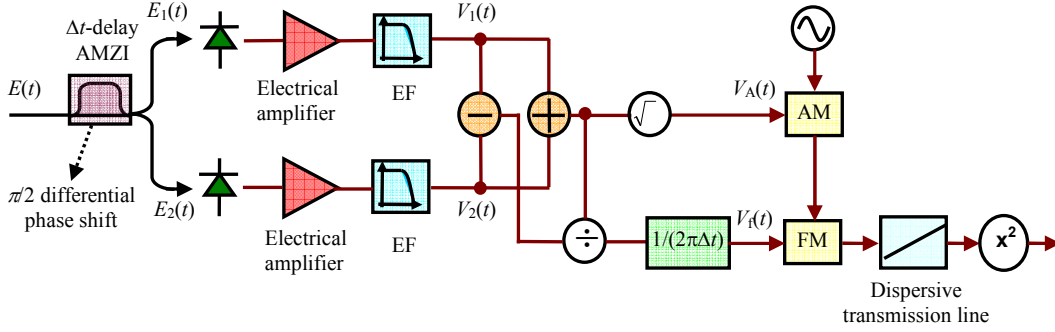


Fig. 1. Principle of full optical-field EDC (AM: Amplitude modulator, FM: Frequency modulator)

sensitivity to the tuning of these parameters. In Section V, the configuration of numerical simulations is presented, and these simulations are used to clarify the observed experimental trends and predict further performance improvement of full-field EDC, as discussed section VI. Finally, Section VII summarizes the results.

II. PRINCIPLE OF FULL-FIELD EDC

Figure 1 depicts the principle of full-field EDC. The incoming optical signal is processed by a single AMZI with a differential time delay of Δt and differential phase shift of $\pi/2$. Assuming that the input optical field (baseband representation) is $E(t)$, the two outputs of the AMZI, $E_1(t)$ and $E_2(t)$, are given by:

$$\begin{aligned} E_1(t) &= (E(t) - E(t + \Delta t)e^{j\pi/2})/2 \approx \\ & E(t + \Delta t/2)e^{j\pi/4} [e^{-j\Delta\omega(t)\Delta t/2 - j\pi/4} - e^{j\Delta\omega(t)\Delta t/2 + j\pi/4}]/2 \\ E_2(t) &= (E(t) + E(t + \Delta t)e^{j\pi/2})/2 \approx \\ & E(t + \Delta t/2)e^{j\pi/4} [e^{-j\Delta\omega(t)\Delta t/2 - j\pi/4} + e^{j\Delta\omega(t)\Delta t/2 + j\pi/4}]/2 \end{aligned} \quad (1)$$

where $\Delta\omega(t) = \omega(t) - \omega_0$ is the instantaneous frequency of baseband representation of the optical field, $E(t)$, and ω_0 is the optical carrier frequency. $E_1(t)$ and $E_2(t)$ are incident on a pair of detectors, electrically amplified, and filtered by electrical filters (EFs) to obtain the electrical signals $V_1(t)$ and $V_2(t)$:

$$\begin{aligned} V_1(t) &= \alpha_1 |E(t + \Delta t/2)|^2 \sin^2(\Delta\omega(t)\Delta t/2 + \pi/4) \\ V_2(t) &= \alpha_2 |E(t + \Delta t/2)|^2 \cos^2(\Delta\omega(t)\Delta t/2 + \pi/4) \end{aligned} \quad (2)$$

where α_1 and α_2 are scaling factors taking account of the responsivities of the detectors and the gains of the electrical amplifiers for the $V_1(t)$ and $V_2(t)$ signal paths. For analytical simplicity, $\alpha_1 = \alpha_2 = 1$ is assumed here. Signals proportional to the amplitude, instantaneous frequency, and phase information of the optical field, $V_A(t)$, $V_f(t)$, and $V_p(t)$, can be extracted by signal processing of $V_1(t)$ and $V_2(t)$:

$$V_A(t) = [V_1(t) + V_2(t)]^{1/2} = |E(t + \Delta t/2)|$$

$$\begin{aligned} V_f(t) &= [V_1(t) - V_2(t)]/[2\pi\Delta t V_1(t) + 2\pi\Delta t V_2(t)] \\ &= \sin(\Delta\omega(t)\Delta t)/(2\pi\Delta t) \approx \Delta\omega(t)/2\pi \\ V_p(t) &= 2\pi \int V_f(\tau) d\tau \end{aligned} \quad (3)$$

where the approximation in the expression for $V_f(t)$ is valid for $\Delta\omega(t)\Delta t \ll 1$. The intensity and frequency information is used to reconstruct a replica of the optical signal in the radio frequency (RF) range by applying the signals V_A and V_f to amplitude and frequency modulators respectively, allowing for subsequent full optical-field compensation using a dispersive transmission line [9]. This scheme offers a compromise between conventional cost-effective DD EDC that lacks phase information and coherent-detection based EDC that has better performance but requires complicated phase and polarisation tracking.

Fig. 1 shows that in principle, a pair of detectors is sufficient to access both the amplitude and phase information. However, as is well known, it is difficult in practice to precisely match the response of two independent receiver chains. Therefore, we adopted an equivalent implementation using a balanced photo-detector to give $V_1 - V_2$ and an additional single photo-detector to obtain $V_1 + V_2$ [10-11].

III. EXPERIMENTAL SETUP

Fig. 2 shows the experimental setup. A 1555.7nm signal from a distributed feedback (DFB) laser was intensity modulated using a Mach-Zehnder modulator (MZM) at 10Gbit/s with a $2^{11}-1$ pseudo random bit sequence (PRBS). The pattern length was selected to facilitate off-line signal processing. The extinction ratio was set to be either 12dB or 6dB by adjusting the bias and the amplitude of the electrical data. The generated OOK signal was transmitted over a recirculating loop comprising 124km of field-installed SSMF in the BT Ireland network between Cork City and Clonakilty, County Cork, Ireland, with a signal launch power of approximately 0dBm per span, at which the fibre nonlinear effect was negligible [10]. The noise figure of the loop amplifiers was 4.5dB.

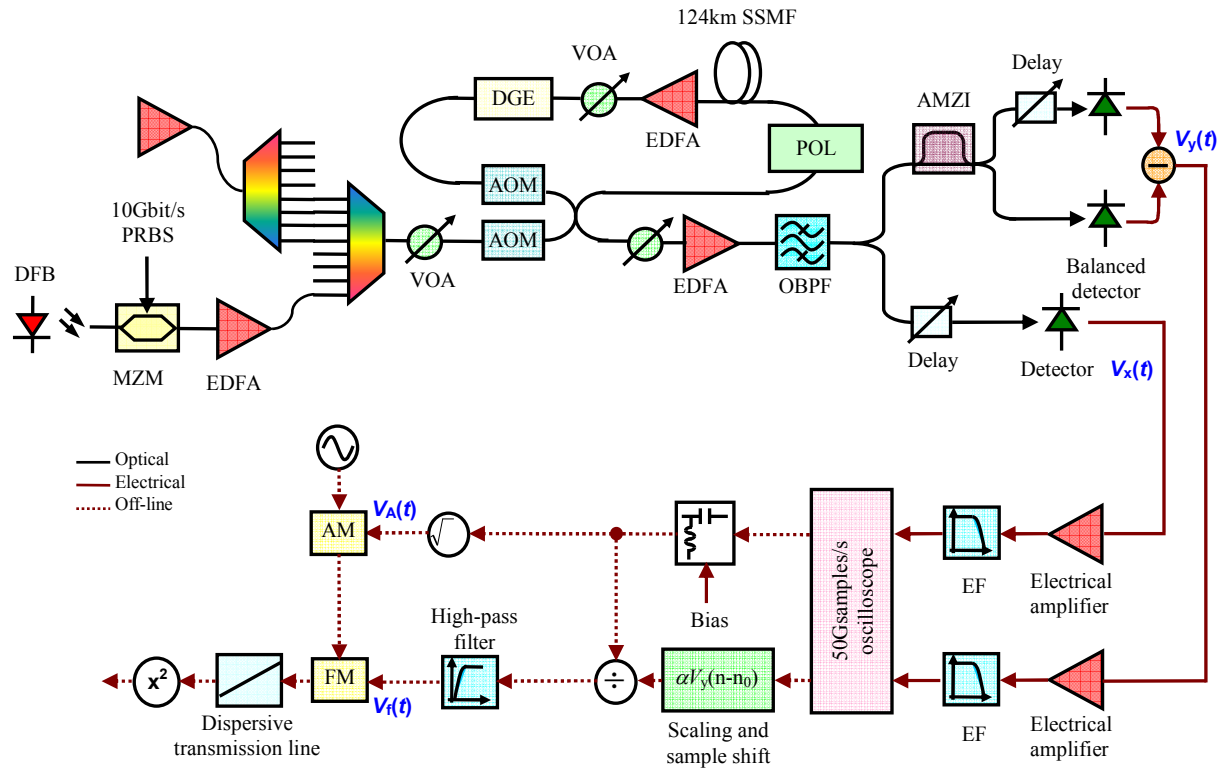


Fig. 2. Experimental setup (VOA: Variable optical attenuator; AOM: Acousto-optic modulator)

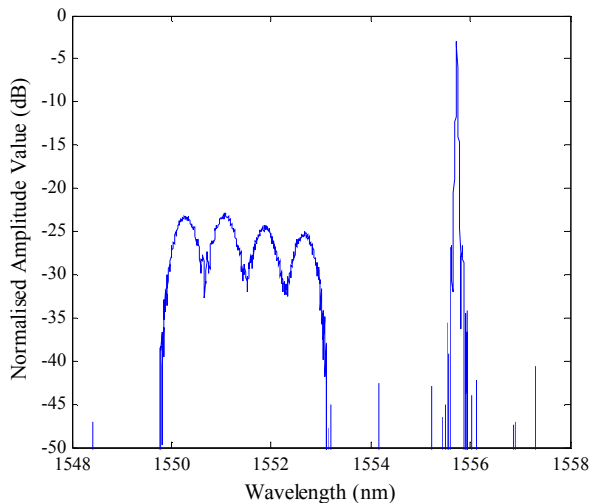


Fig. 3. Spectrum of launched signal and co-propagated ASE noise

The signal polarisation was randomised after each recirculation using an Adaptif A3200-1 synchronous polarisation scrambler (POL). A 3nm-wide band (1550-1553nm) of ASE noise, with spectral power density 20dB less than that of the signal, co-propagated with the signal to ensure that the loop amplifier was appropriately saturated. The ASE noise was obtained from an erbium doped fibre amplifier (EDFA) filtered by an eight-channel arrayed waveguide grating (AWG), as shown in Fig. 2. A dynamic gain equaliser (DGE) was used in the loop to compensate

for residual amplifier gain tilt. The spectrum of the signal and the ASE noise launched into the loop is shown in Fig. 3.

At the receiver, the signal was pre-amplified and optically filtered by either a 0.8nm (as used in [11]) or a 0.3nm optical bandpass filter (OBPF). Ten percent of the signal power was detected by a 10GHz single photo-detector and electrically amplified with a 12GHz bandwidth. The remaining signal was optically processed by an AMZI with 11.76ps (free spectral range (FSR) of 85GHz) time delay and $\pi/2$ phase shift, detected by a 40GHz balanced detector, and electrically amplified with a net amplification bandwidth of 15GHz. The use of 40GHz balanced detector for 10Gbit/s signal detection was restricted by our equipment availability, and the bandwidth of this path was limited by the following electrical amplifiers. The detected signals from the single and balanced photo-detectors, represented by $V_x(t)$ and $V_y(t)$, were sampled by a real-time oscilloscope at a sampling rate of 50Gsamples/s. Off-line processing of one million bits (five million samples) was used for optical intensity and phase recovery. The relative delays of the three signal paths shown in Fig. 2 were fine tuned using optical delays placed prior to the detectors.

In the subsequent off-line processing, $V_x(t)$ (electrical signal from the single photo-detector) was re-biased to allow for the AC coupling of the receiver and to increase the robustness to thermal noise [10-11]. To allow for coarse path length mismatch, a sample shifting was included in the $V_y(t)$ (electrical signal from the balanced detector) path to

provide delay tunability with a resolution equivalent to the sampling interval (20ps), and the amplitude was adjusted to correct for any gain imbalance. A Gaussian-shaped high-pass (HP) electrical filter with 1GHz 3dB cut-off frequency was employed (unless otherwise stated) to suppress the effect of low-frequency component amplification [10]. The recovered intensity and phase were employed to reconstruct a full optical field at base band, which was compensated by multiplying an inverse transfer function of the CD in the fibre link. The compensated signal was square-law detected and decoded using optimal threshold detection to calculate the bit error rate (BER) by direct error counting.

IV. EXPERIMENTAL RESULTS

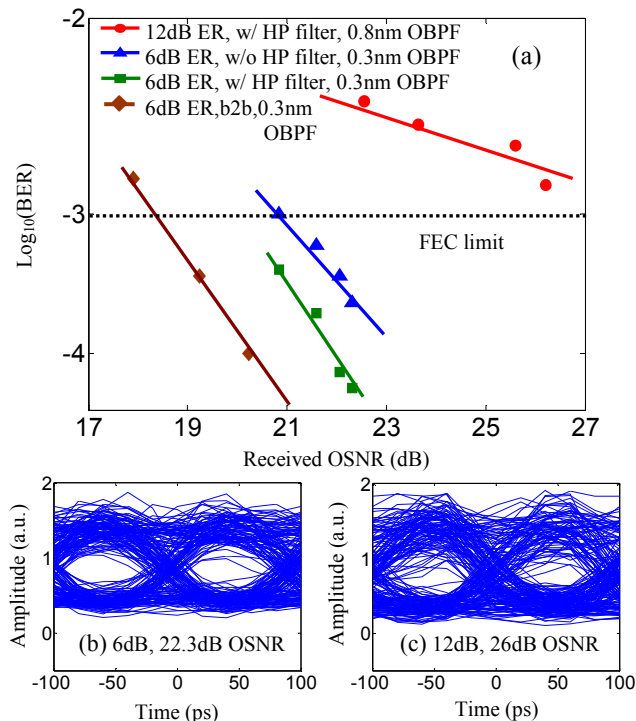


Fig. 4(a). $\log_{10}(\text{BER})$ versus received OSNR after 496km SSMF transmission. (b) and (c): Reconstructed eye diagrams with high pass filtering (b) at 22.3 dB OSNR with 6dB ER and 0.3nm OBPF and (c) at 26dB OSNR with 12dB ER and 0.8nm OBPF.

Figure 4(a) illustrates the performance of full-field EDC for a 12dB signal extinction ratio (ER) and 0.8nm OBPF (circles), and 6dB signal ER and 0.3nm OBPF (squares), after 496km SSMF transmission. The diamonds represent the back-to-back case using 0.3nm OBPF and 6dB signal ER. To show the influence of the high-pass electrical filter, the BER versus received optical signal to noise ratio (OSNR) without a high-pass electrical filter for the case of 6dB ER and 0.3nm OBPF is also plotted (triangles). The insets show the eye diagrams of compensated signal (b) at 22.3dB OSNR using 6dB ER and 0.3nm OBPF; (c) at 26dB OSNR using 12dB ER and 0.8nm OBPF. From the figure, it may be observed that 496km was not achievable using 12dB ER and a 0.8nm OBPF. This was because ASE noise

was not properly suppressed by the relatively wide bandwidth of the OBPF. Such noise not only directly degraded the quality of the photodiode outputs but also severely affected full-field reconstruction via the electronic amplification of the signal noise arising from the division by the total received power in phase estimation (Fig. 2) and low-frequency amplification [10]. By using a 6dB signal ER and 0.3nm OBPF, significant performance improvement was obtained, and the OSNR penalty, compared to the back-to-back case, was less than 2dB. This improvement is primarily attributed to a reduction of ASE noise due to narrower bandwidth of the OBPF. Note that whilst the 0.3nm OBPF greatly suppressed the ASE noise, the optimum filter width is narrower ($\sim 0.1\text{nm}$), as will be shown in Section VI. The resultant excess noise associated with the 0.3nm OBPF increased the significance of the noise amplification process which in turn impacted the optimum ER. Consequently, a reduced ER of 6dB would result in the minimum value of sampled version of $V_x(t)$ being increased, greatly suppressing the noise amplification arising from the division of $V_x(t)$ in the estimation of $V_R(t)$.

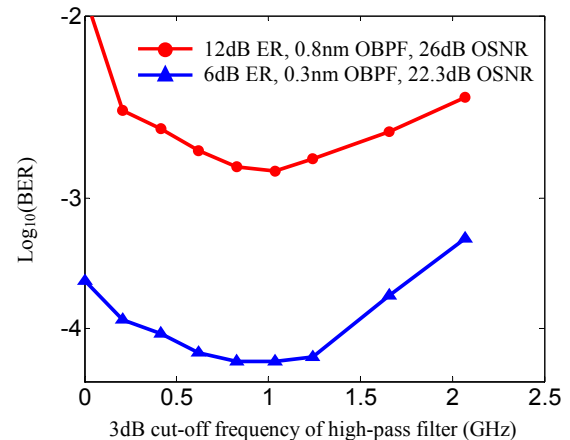


Fig. 5. $\log_{10}(\text{BER})$ versus cut-off frequency of high-pass filter. Circles: 12dB signal ER, 0.8nm OBPF, 26dB OSNR; Triangles: 6dB signal ER, 0.3nm OBPF, 22.3dB OSNR.

The use of a high-pass filter during full-field reconstruction can suppress the low-frequency component amplification and improve the compensated signal quality, as shown in Fig. 5. The level of improvement afforded by the high-pass filter was clearly dependent on the noise level, and in the case of 6dB ER with a 0.3nm OBPF where the noise has already been significantly suppressed, the benefit of the high-pass filter was not prominent. However, when the noise level was not properly reduced (in the case of 12ER and 0.8nm OBPF), it was essential to use a high-pass filter to suppress low-frequency amplification of the noise. As a result, BER exhibited over one order of magnitude increase when the filter was removed. The figure also shows that the optimal cutoff frequency of the filter was around 1GHz for both ERs.

The results described above were obtained when the parameters in off-line processing, including the bias added

to $V_x(t)$ and the compensation ratio, were optimised. However, the sensitivity of the system to these parameters could affect the practicality of the technique. Fig. 6 shows performance variation as a function of (a) normalized bias coefficient M and (b) effective compensation length, where the bias (Fig. 2) was calculated to be $-M \cdot \min(V_x(t))$ and the dispersion coefficient of the dispersive transmission line was scaled to an equivalent length of SSMF with 16ps/km/nm dispersion. The ER was 6dB and OBPF had 3dB bandwidth of 0.3nm. Note that due to AC coupling of the receiver, $\min(V_x(t))$ had a negative value. From the figure, it may be seen that for proper operation of full-field EDC, it is essential to bias the sampled values of $V_x(t)$ to a value larger than zero ($M > 1$). This is because $V_f(t) = V_y(t)/(V_x(t) + \text{bias})$ has a π phase shifts whenever $V_x(t) + \text{bias}$ changes sign. When the noise amplification due to division by $V_x(t) + \text{bias}$ is suppressed ($M > 1$), the system performance is robust to further bias increase. The optimal bias value balances the noise amplification and bias induced distortion to the estimated frequency.

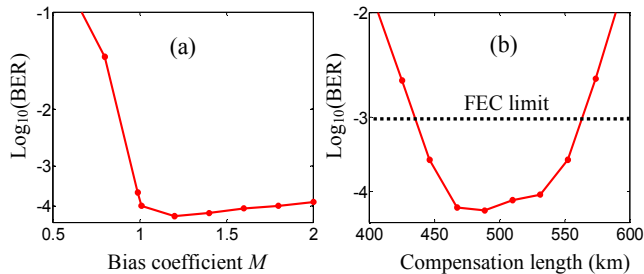


Fig. 6. $\log_{10}(\text{BER})$ as a function of (a) bias coefficient M and (b) compensation length for 6dB ER and 0.3nm OBPF after 496km SSMF transmission.

Fig. 6(b) illustrates the tolerance to errors in the estimation of CD compensation. It is shown from the figure that the tolerance range at 496km using full-field EDC is comparable to that of a signal measured back-to-back without EDC. At the FEC limit (BER of 10^{-3}), the tolerance range is around 120km.

Finally, we investigated possible simplification of the off-line processing setup in Fig. 2 by omitting the division of $V_x(t)$ which contributes to the ER and ASE sensitivity of the system. This simplification would greatly reduce the complexity of the system in practice because the intensity and phase estimation paths could be independently processed without synchronization until they reach the amplitude and frequency modulators in Fig. 2. The system parameters used for this investigation were those obtained by optimization with the divider in place. This omitting of the divider resulted in a small OSNR penalty of around 1dB at BER of 10^{-3} as shown in Fig. 7, which depicts the performance with (squares) and without (triangles) the division. This is in close agreement to previously simulated performance which indicated a 1dB Q -factor degradation at 500km with an 83km amplifier spacing [9]. Furthermore, there is no sign of error floor for the measured data without

the divider (OSNR value up to 22.3dB). At 496km and 22.32dB OSNR, a BER of 10^{-3} could still be achieved while implementation complexity was reduced, and further improvement is anticipated for a system optimized for this processing algorithm.

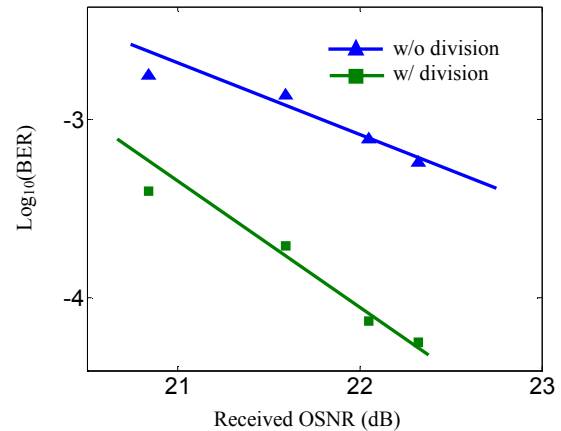


Fig. 7. $\log_{10}(\text{BER})$ versus received OSNR with (squares) and without (triangles) the division of $V_x(t)$. ER is 6dB and OBPF bandwidth is 0.3nm. A 1GHz Gaussian-shaped high-pass filter is used.

V. SIMULATION SETUP

In section IV, it is shown that the performance of a full-field EDC system can be improved by using a narrower OBPF and a reduced ER, and 492km field-installed SSMF transmission with a reduced BER at a lower OSNR of 22dB can be achieved (compared to our previous work [11]). In Section VI, we present results from numerical optimization of the system which provide critical design criteria for maximising the transmission reach of our system. The simulation model used in this paper matches the experiment setup in Fig. 2 except that instead of using a recirculating fibre loop, the transmission link consisted of cascaded spans with 120km SSMF per span and no ASE noise was co-propagated with the signal. Details are as follows. Continuous wave light was intensity modulated by a 10Gbit/s OOK data train using an MZM. The data train consisted of a $2^{11}-1$ PRBS repeated nine times (18,423 bits). Ten '0' bits and eleven '0' bits were added before and after this data train respectively to simplify the boundary conditions. The bits were raised-cosine shaped with a roll-off factor of 0.4 and 40 samples per bit. The ER of the modulated OOK signal was set by adjusting the bias and the amplitude of the electrical OOK data.

The signal was launched into the transmission link of 120km SSMF per span with 0dBm [10]. The SSMF was assumed to have CD of 16ps/km/nm, a nonlinear coefficient of $1.2/W/\text{km}$, and a loss of 0.2dB/km. The split-step Fourier method was used to calculate the signal propagation in the fibers. At the end of each span, noise from optical amplifiers was modelled as complex additive white Gaussian noise with zero mean and a power spectral density of $n_{sp} h \nu (G-1)$ for each polarisation, where G is the amplifier

gain, $h\nu$ is the photon energy, and n_{sp} is the population inversion factor of the amplifiers which was set to give 4dB amplifier noise figure (NF).

The noise of the optical preamplifier was also modelled as additive white Gaussian noise with random polarisation. The launch power into the preamplifier was adjusted to control the OSNR. The pre-amplified signal was filtered by a Gaussian-shaped OBPF. The signal after the OBPF was then split into two paths to extract $V_x(t)$ and $V_y(t)$, as shown in Fig. 2. The AMZI for the extraction of $V_y(t)$ had $\pi/2$ differential phase shift and 10ps differential time delay. The responsivities of the balanced and single photo-detectors were assumed to be 0.6A/W and 0.9A/W respectively, and equivalent thermal noise spectral power densities were assumed to be 100pA/Hz^{1/2} and 18pA/Hz^{1/2} respectively. These receiver parameters match typical values of the commercial detectors used in the experimental demonstration above. A received power of 0dBm was assumed for each detector. After detection, the signals were electrically amplified, filtered by 15GHz 4th-order Bessel electrical filters, and down-sampled to 50Gsamples/s (5 samples per bit at 10Gbit/s) to simulate the sampling effect of the real-time oscilloscope. The down-sampled copy of $V_x(t)$ was re-biased and a Gaussian-shaped high-pass EF, to suppress the impairment from low-frequency component amplification, was included. The extracted information was used to reconstruct a replica of the optical signal, which was subsequently compensated using a dispersive transmission line. The compensated signal was then square-law detected and decoded using optimal threshold detection.

The simulation was iterated 10 times with different random number seeds to give a total of 184,320 simulated bits. The performance was evaluated in terms of the required OSNR to achieve a BER of 5×10^{-4} by direct error counting. 184,320 bits were sufficient to produce a confidence interval of $[3.5 \times 10^{-4} \ 7 \times 10^{-4}]$ for this BER with 99% certainty [14].

VI. SIMULATION RESULTS

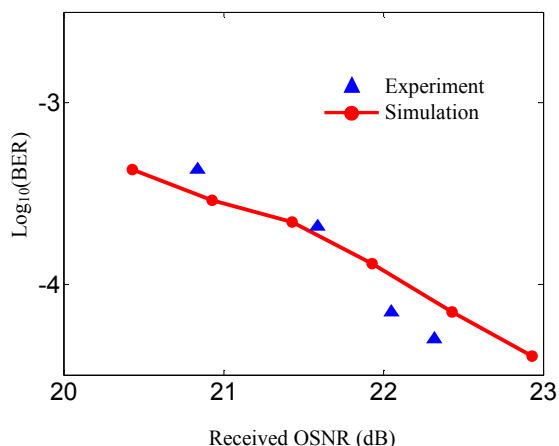


Fig. 8. $\log_{10}(\text{BER})$ versus received OSNR for simulations (solid lines) and experiments. ER is 6dB and OBPF bandwidth is 0.3nm.

Fig. 8. shows the comparison of the simulation and experimental results. The simulation was carried out with parameters set as closely as possible to the experimental parameters. The figure shows a very good match between the experiment and the simulation. Note that these parameters were not optimized. The performance sensitivity to system parameters to enable optimal performance of full-field EDC will be investigated as follows.

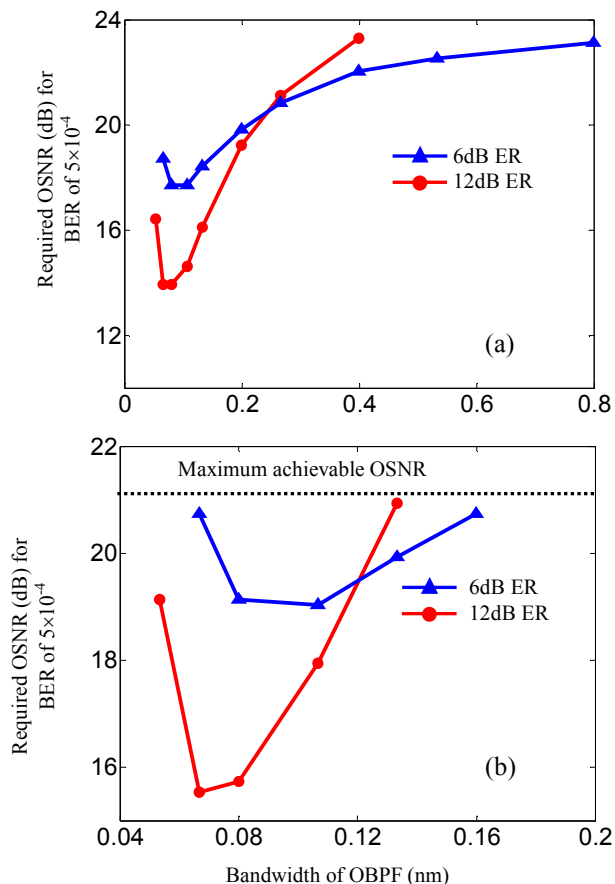


Fig. 9. Required OSNR versus 3dB bandwidth of OBPF at 6dB ER (triangles) and 12dB ER (circles) for (a) 480km and (b) 960km.

Fig. 9 shows required OSNR as a function of OBPF bandwidth at 6dB and 12dB ER for (a) 480km and (b) 960km. A 0.85GHz high-pass electrical filter was used for suppression of low-frequency component amplification. From Fig. 9(a), it is shown that when the ASE noise was not sufficiently suppressed (bandwidth > 0.2nm), a system with 6dB signal ER exhibited better performance compared to that with 12dB ER. As described above, this is because a lower ER effectively reduced noise amplification arising from the division by total received power and low-frequency amplification in phase estimation. However, if the ASE noise was sufficiently suppressed (bandwidth < 0.2nm), the benefit of reducing the ER was greatly reduced. Clearly, the optimal performance depended on the balance between mitigating the noise amplification and penalty induced by a lower ER. The optimal filter bandwidth for both ERs was around 0.1nm, at which the required OSNR was only 14dB at BER of 5×10^{-4} by using a

12dB ER. In Fig. 9(b), it is shown that for the optimized OBPF bandwidth, 960km transmission reach was also achieved, albeit with a substantially reduced tolerance in OBPF bandwidth.

The capability of full-field EDC to compensate fibre length up to 1000km was further verified in Fig. 10(a). In this figure, it is shown that with 12dB ER and 0.07nm OBPF, the required OSNR to achieve a transmission distance of 1200km was around 18dB. Such narrow OBPF is achievable by using fibre Bragg grating (FBG) [15]. Note that the use of such narrow-bandwidth filter would tighten the requirement for laser wavelength stabilization and may need dynamic wavelength tracking to facilitate device aging and wavelength drift.

As discussed in section IV, a system with 12dB signal ER, compared to that with a 6dB ER, was more sensitive to low-frequency amplification and thus the bandwidth of Gaussian-shaped high-pass electrical filter. The optimal high-pass filter bandwidth was found to be around 0.85GHz at 12ER and 960km, as depicted in Fig. 10(b), beyond which distortions induced by high-pass electrical filter dominated.

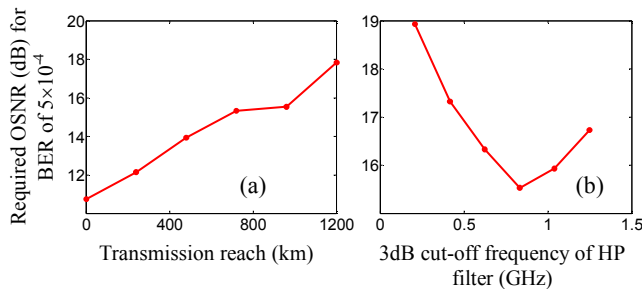


Fig. 10. (a) Required OSNR versus fibre length at 12dB ER. The high-pass filter is 0.85GHz. (b) Required OSNR versus 3dB cut-off frequency of high-pass filter at 960km. The OBPF bandwidth is 0.07nm.

From previous simulations, we have shown that it is essential to balance noise amplification, arising from the division by total received power $V_x(t)$ and low-frequency amplification, and penalty induced by a lower ER. However, the effect of thermal noise was not explicitly investigated, which would also be increased by noise amplification mechanisms in phase estimation. Although the optical power at the receiver could be relatively high (e.g. 0dBm), the power of $V_y(t)$ from the output of the AMZI depends on the differential time delay Δt :

$$V_y(t) \propto |E(t)|^2 \Delta \omega(t) \Delta t + n_{th-y} \quad (4)$$

Therefore, for small Δt , thermal noise could play an important role even for high signal powers and can be even more severe than ASE noise for sufficiently small time delay. The differential time delay must therefore be properly designed between values favouring linear estimation of the instantaneous frequency and thermal noise. The maximum achievable OSNR itself may be enhanced either by use of Raman amplification or by reducing the amplifier spacing. To examine the ultimate reach of full-field EDC, we therefore assumed that the signal had 12dB

ER and -3dBm signal launch power per span, and the fibre length per span was 80km. The bandwidth of the OBPF and the cut-off frequency of the high-pass electrical filter were fixed at the optimized values for the case of 30ps AMZI DTD at 2160km. In a separate investigation, we observed that the optimum parameter values do not vary significantly with the fibre lengths. Other parameters were the same as those in the previous simulation.

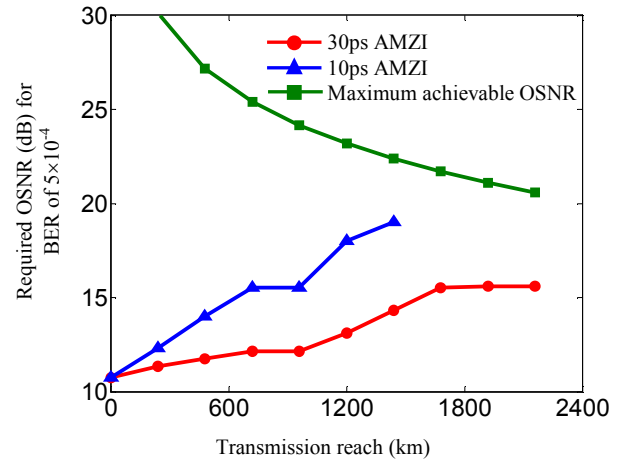


Fig. 11. Required OSNR as a function of fibre length for AMZI time delay of 30ps (circles) and 10ps (triangles). Squares represent the maximum achievable OSNR. The OBPF bandwidth is 0.07nm and the HP filter cut-off frequency is 0.85GHz. The ER is 12dB.

Fig. 11 shows the performance versus transmission distance for AMZI time delay of 30ps and 10ps. Squares represent the maximum achievable OSNR of the system. It is clearly shown that an AMZI with larger time delay could greatly improve the performance and allow 2160km transmission with 15.7dB required OSNR. 80km amplifier spacing and -3dBm signal launch power per span provided improved maximum achievable OSNR resulting in a predicted OSNR margin of 5dB at 2160km. Note that the results above assumed a sampling rate of 50Gsamples/s. When reducing the sampling rate to 20Gsamples/s, around 1.2dB and 5dB OSNR penalties were induced for the fibre length of 480km and 2160km respectively [10].

VII. CONCLUSION

We have experimentally demonstrated full-field EDC technique to achieve a bit error rate of 5×10^{-5} at 22.3dB OSNR for 10Gbit/s OOK signal after 4 spans of 124km (496km total length) field-installed SSMF. This was achieved by effectively suppressing the impact of ASE noise and the associated electronic amplification of the noise during full-field reconstruction. We also investigated performance sensitivity to signal processing parameters. Numerical simulations were performed to estimate the maximum reach for this technique, resulting in a prediction of single-channel transmission distance of 2160km with 80km per span without need for optical compensation.

ACKNOWLEDGEMENT

The authors gratefully acknowledge BT Ireland, particularly J.Coleman, M.Conroy, W.McAuliffe, R.O'Regan and M.O'Reilly, for providing access to the fibre link.

REFERENCES

- [1] T. Ellermeyer, J. Mullrich, J. Rupeter, H. Langenhagen, A. Bielik, and M. Moller, "DA and AD converters for 25 GS/s and above," *IEEE/LEOS Summer Topical Meetings*, pp. 117-118, 2008.
- [2] J. Weem, P. Kirkpatrick, and J. Verdiell, "Electronic dispersion compensation for 10 Gigabit communication links over FDDI legacy multimode fibre," *Optical Fibre Communication Conference (OFC)*, paper OFO4, 2005.
- [3] A. Polley and S.E. Ralph, "Receiver-side adaptive opto-electronic chromatic dispersion compensation," *Optical Fibre Communication Conference (OFC)*, paper JThA51, 2007.
- [4] T. Kupfer, C. Dorschky, M. Ene, and S. Langenbach, "Measurement of the Performance of 16-States MLSE Digital Equalizer with Different Optical Modulation Formats," in *Optical Fiber Communication Conference and Exposition and The National Fiber Optic Engineers Conference*, OSA Technical Digest (Optical Society of America, 2008), paper PDP13.
- [5] M.D. Feuer, Sun-Yuan Huang, S.L. Woodward, O. Coskun, and M. Boroditsky, "Electronic dispersion compensation for a 10-Gb/s link using a directly modulated laser," *Photonics Technology Letters, IEEE*, vol. 15, pp. 1788-1790, 2003.
- [6] J. McNicol, M. O'Sullivan, K. Roberts, A. Comeau, D. McGhan, and L. Strawczynski, "Electrical domain compensation of optical dispersion," *Optical Fibre Communication Conference (OFC)*, OThJ3, 2005.
- [7] S.J. Savory, G. Gavioli, R.I. Killey, and P. Bayvel, "Electronic compensation of chromatic dispersion using a digital coherent receiver," *Opt. Express*, vol. 15, pp. 2120-2126, 2007.
- [8] G. Charlet, M. Salsi, H. Mardoyan, P. Tran, J. Renaudier, S. Bigo, M. Astruc, P. Sillard, L. Provost, and F. Cerou, "Transmission of 81 channels at 40Gbit/s over a transpacific-distance erbium-only link, using PDM-BPSK modulation, coherent detection, and a new large effective area fibre," *European Conference on Optical Communications (ECOC)*, PDP Th3.E.3, 2008.
- [9] M.E. McCarthy and A.D. Ellis, "Low-cost receiver side electronic dispersion compensation of the full optical field," *Optical Fibre Communications and Electronic Signal Processing, The IEE Seminar on (Ref. No. 2005-11310)*, 2005, pp. 0_16-3/6.
- [10] J. Zhao, M.E. McCarthy, and A.D. Ellis, "Electronic dispersion compensation using full optical-field reconstruction in 10Gbit/s OOK based systems," *Opt. Express*, vol.16, pp. 15353-15365, 2008.
- [11] J. Zhao, M.E. McCarthy, P. Gunning, and A.D. Ellis, "Pattern sensitivity in electronic dispersion compensation using full optical-field reconstruction", *Asia-Pacific Optical Conference (APOC)*, paper 7136-82, 2008.
- [12] M.E. McCarthy, J. Zhao, P. Gunning, and A.D. Ellis, "A novel field-detection maximum-likelihood sequence estimation for chromatic dispersion compensation", *European Conference on Optical Communications (ECOC)*, paper We.2.E.5, Brussels, Belgium, 2008.
- [13] J. Zhao, M.E. McCarthy, P. Gunning, and A.D. Ellis, "Chromatic dispersion compensation using full optical-field maximum likelihood sequence estimation", *Optical Fibre Communication Conference (OFC)*, paper OThE6, 2009.
- [14] M. Jeruchim, "Techniques for Estimating the Bit Error Rate in the Simulation of Digital Communication Systems," *Selected Areas in Communications, IEEE Journal on*, vol. 2, pp. 153-170, 1984.
- [15] J.D. Downie, J. Hurley, M. Sauer, S. Lobanov, and S. Raghavan, "Experimental measurements of the effectiveness of MLSE against narrowband optical filtering distortion," *Optical Fibre Communication Conference (OFC)*, paper OMG4, 2007.

Mary McCarthy was born in Mallow, Ireland and gained a B.Eng in Electrical and Electronic Engineering from University College Cork, Cork, Ireland in 2004.

She is currently with the Photonic Systems Group at the Tyndall National Institute in Cork, Ireland where her research interests include the application of electronic signal processing to optical communication systems.

Dr Jian Zhao received a B.Eng degree from University of Science and Technology of China (USTC) in 2002, M.Phil. and Ph.D. degrees from the Chinese University of Hong Kong (CUHK) in 2004 and 2007 respectively. He joined the Photonic Systems Group at the Tyndall National Institute as a Postdoctoral Research Scientist in August 2007. His current research interests include electronic signal processing in optical communications and spectrally-efficient multi-carrier optical transmission systems.

Dr Zhao is a member of IEEE and is an Enterprise Ireland principal investigator. He was the recipient of the First Prize of Outstanding Student Scholarship of USTC. He has published more than 30 technical papers in peer-reviewed international journals and conferences and 1 patent.

Dr. Andrew Ellis was born in Underwood, England in 1965 and gained a BSc in Physics with a minor in mathematics from the University of Sussex, Brighton, England in 1987. He was awarded his PhD in Electronic and Electrical Engineering from The University of Aston in Birmingham, Birmingham, England in 1997 for his study on All Optical Networking Beyond 10Gbit/s.

He previously worked for British Telecom Research Laboratories as a Senior Research Engineer investigating the use of optical amplifiers and advanced modulation formats in optical networks and the Corning Research Centre as a Senior Research Fellow where he led activities in optical component characterisation. Currently, he heads the Transmission and Sensors Group at the Tyndall National Institute in Cork, Ireland, where he is also a member of the Department of Physics, University College Cork. He research interests include the evolution of core and metro networks, and the application of photonics to sensing.

Dr Ellis is a member of the Institute of Physics and the Institute of Engineering Technology, and is a Chartered Physicist. He acts as a reviewer for IEEE Journal of Lightwave Technology and Photonics Technology Letters and has published over 100 journal papers and over 20 patents in the field of Photonics.

Dr. Paul Gunning joined BT Laboratories in 1994 to investigate high-speed all-optical networks and photonic packet switching. In 1998 he moved to BT's Futures Testbed where he works on Ethernet, router performance testing, Layer 2/Layer 3 MPLS VPNs and reconfigurable optical networks. Paul graduated with a B.Sc. in Applied Physics from Dublin City University in 1992. He was awarded an M.Sc. in laser physics and a Ph.D in photonic switching networks from Essex University in 1995 and 2001 respectively.